Letter   Editors' Suggestion

Magnetic structure and spin fluctuations in the colossal magnetoresistance ferrimagnet Mn₃Si₂Te₆

Feng Ye ⓘ,[1,*] Masaaki Matsuda ⓘ,[1] Zachary Morgan ⓘ,[1] Todd Sherline ⓘ,[1] Yifei Ni ⓘ,[2] Hengdi Zhao ⓘ,[2] and G. Cao ⓘ[2]

[1]*Neutron Scattering Division, Oak Ridge National Laboratory, Oak Ridge, Tennessee 37831, USA*
[2]*Department of Physics, University of Colorado at Boulder, Boulder, Colorado 80309, USA*

The ferrimagnetic insulator $Mn_3Si_2Te_6$, which features a Curie temperature T_c at 78 K and a delicate yet consequential magnetic frustration, exhibits colossal magnetoresistance (CMR) when the magnetic field is applied along the magnetic hard axis, surprisingly inconsistent with existing precedents [Y. Ni, H. Zhao, Y. Zhang, B. Hu, I. Kimchi, and G. Cao, Phys. Rev. B **103**, L161105 (2021)]. This discovery motivates a thorough single-crystal neutron diffraction study in order to gain insights into the magnetic structure and its hidden correlation with the new type of CMR. Here we report a noncollinear magnetic structure below the T_c where the moments lie predominantly within the basal plane but tilt toward the c axis by $\approx 10°$ at ambient conditions. A substantial magnetic diffuse scattering decays slowly and persists well above the T_c. The evolution of the spin correlation lengths agrees well with the electrical resistivity, underscoring the role of spin fluctuation contributing to the magnetoresistivity near the transition. Application of magnetic field along the c axis renders a swift occurrence of CMR but only a slow tilting of the magnetic moments toward the c axis. The unparalleled changes indicate a nonconsequential role of magnetic polarization.

Colossal magnetoresistance (CMR), the dramatic change in electric resistance in response to an applied magnetic field, has been known for decades and is extensively studied in the archetypical perovskite manganites and their variants [1]. In these systems, the simultaneous insulator-metal transition and the ferromagnetic order of the mixed Mn^{3+}-Mn^{4+} network can be understood in the context of the "double exchange" mechanism; the electron hopping is enhanced when neighboring Mn ions have mutually aligned spins [2–4]. The spin order promotes the electron hopping and increases the effective exchange interaction, annealing out the lattice distortion, thus leading to the insulator-metal transition.

Exploring new classes of materials exhibiting CMR beyond the perovskite manganites continues to inspire huge interest, as they expand the option for optimizing magnetoresistive properties for applications like spintronic devices with low dissipation. The discovery of the large enhancement of magnetoresistance in Sc-doped pyrochlores $Tl_2Mn_2O_7$ [5–7] with the same oxidation state of the Mn ion and essentially unchanged transition temperature T_c suggests a new paradigm for manipulating magnetoresistance. A theoretical model attributed the CMR phenomena in $Tl_{2-x}Sc_xMn_2O_7$ to magnetic polarons formed above the T_c as the carrier concentration is sufficiently low [8]. It is proposed that the magnetic fluctuations generate an effective static potential that scatters the carriers and gives rise to electric resistance. The fact that low-field magnetoresistance scales well with carrier densities over two orders of magnitude and in materials with different magnetic models reveals a ubiquitous relationship between the magnetoresistivity and charge carrier density in ferromagnetic metals and doped semiconductors [9].

Despite these differences between the perovskite and pyrochlore manganites, an essential element these materials and all other CMR materials commonly share is magnetic polarization, which minimizes spin scattering and thus electrical resistance. However, the ferrimagnet $Mn_3Si_2Te_6$ is a surprising exception to this rule. The recently discovered CMR in this material is realized only when the magnetic polarization is avoided [10]. The inherent frustration due to competing exchange interactions between neighboring Mn ions prevents the formation of a long-range order until the temperature is lowered to $T_c = 78$ K [11,12,14]. The large linear term in the heat capacity confirms critical magnetic fluctuations arising from the competing exchange interactions, which may hold the key to understanding the CMR [10]. $Mn_3Si_2Te_6$ has a magnetic easy axis within the basal plane and a magnetic hard axis along the c axis [12]. The CMR occurs only when the magnetic field, H, is applied along the c axis and it is absent when H is applied within the basal plane. This specific character was later confirmed in a separate study, in which the CMR is attributed to the formation of the nodal-line structure of the valence Te band [15]. Nevertheless, an adequate understanding cannot be established without a thorough microscopic identification of the spin structure, which is conspicuously lacking. In this Letter, we present a comprehensive neutron diffraction characterization of the spin structure as functions of temperature and magnetic field applied along the c axis where the CMR takes place. This Letter uncovers a noncollinear magnetic structure with the magnetic moments predominately lying within the basal plane but tilting toward the c axis by $\approx 10°$ and a strong spin fluctuation persistent well above T_c which the electrical resistivity closely tracks. Application of magnetic field along the c axis only slowly tilts the spins toward the c axis but retains the underlying antiferromagnetic (AFM) configuration.
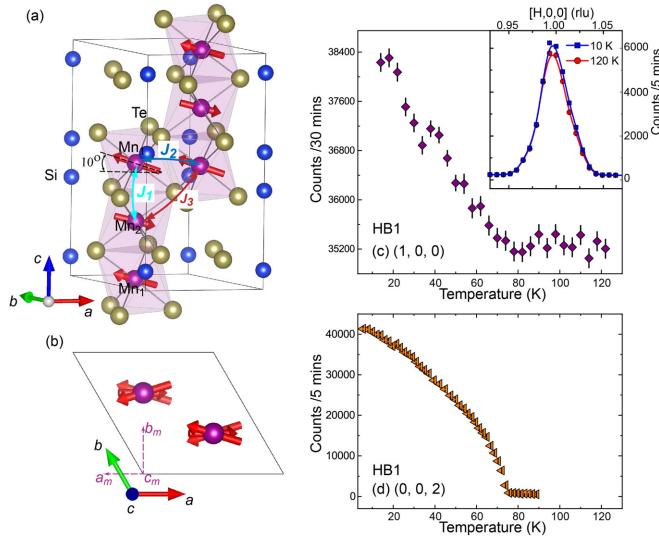
---

*yef1@ornl.gov

FIG. 1. (a) The refined zero-field magnetic structure of $Mn_3Si_2Te_6$ at 5 K. Two symmetry inequivalent Mn sites are located at $(1/3, 2/3, z)$ with $z \approx 0$ and $1/4$. The spin directions are dominantly along the $[1,0,0]$ direction and $\approx 10°$ tilting away from the basal plane. The pathways of the first three AFM exchange interactions $J_1 \approx -402$, $J_2 \approx -73$, and $J_3 \approx -172$ K/Mn [12] between neighboring magnetic ions are also shown in cyan, blue, and red arrows. (b) The magnetic structure projected in the basal plane. a_m, b_m, and c_m are the axes in the monoclinic setting. (c) The T dependence of the $(1,0,0)$ peak associated with the canted spin configuration. Inset: Comparison of the wave-vector scan at 10 and 120 K across the $(1,0,0)$ Bragg peak. (d) The T dependence of the dominant $(0,0,2)$ magnetic peak for the ferrimagnetic spin order.

Single crystals of $Mn_3Si_2Te_6$ were grown using a flux method similar to that in Refs. [10,12,16]. The structural information of the crystal was investigated using a Rigaku XtaLAB PRO diffractometer equipped with a HyPix-6000HE detector. A molybdenum anode was used to generate x rays with wavelength $\lambda = 0.7107$ Å. The samples were cooled by cold nitrogen flow provided by an Oxford N-Helix cryosystem. A single crystal with dimensions of $2 \times 2 \times 0.5$ mm³ was chosen for the diffraction study using the HB1 triple axis spectrometer at the High Flux Isotope Reactor (HFIR) and the CORELLI diffractometer at the Spallation Neutron Source (SNS), all at Oak Ridge National Laboratory (ORNL). The sample was aligned in the $[H, H, L]$ and $[H, 0, L]$ scattering planes for the zero-field study using a closed cycle refrigerator, and subsequently in the $[H, K, 0]$ scattering plane to study the field-dependent evolution of the spin configuration using a 5-T superconducting magnet. The same single crystal was also used for *in situ* neutron diffraction studies with in-plane current applied.

$Mn_3Si_2Te_6$ has a layered structure with trigonal symmetry (SG 163, $P\bar{3}1c$) [12,17,18]. There are two inequivalent Mn_1 and Mn_2 sites in the unit cell. The $MnTe_6$ octahedra are composed of Mn_1 ions that form an edge-sharing honeycomb lattice in the ab plane, while the $MnTe_6$ octahedra consisting of Mn_2 sites form a triangular-lattice sandwiched between the honeycomb layers [Fig. 1(a)]. This leads to a magnetically frustrated network of Mn ions with three dominant

antiferromagnetic exchange interactions [12,14]. The nearest neighbor (NN) exchange interaction J_1 is between the Mn_1 ion of the honeycomb layer and the Mn_2 ion of the triangular layer with bond distance 3.541(1) Å, the next NN coupling J_2 is between the Mn ions within the basal plane with bond distance 4.056(1) Å, and the third NN exchange interaction (J_3) is for Mn ions across the plane with bond distance 5.401(1) Å (all bond lengths are measured at 250 K). $Mn_3Si_2Te_6$ orders ferrimagnetically below $T_c \approx 78$ K [11,12]. There is no structural transition or obvious lattice constant anomaly across the T_c. Details are given in Supplemental Material [13].

Although the crystal maintains the same structural symmetry across the transition, the magnetic configuration cannot be described using any of the four maximal magnetic space groups with the hexagonal lattice. A lower monoclinic magnetic space group $C2'/c'$ (no. 15.89, Belov-Neronova-Smirnova setting [19]) correctly describes the spin configuration at a base temperature of 5 K. The transformation from the hexagonal to monoclinic structure is obtained by $\mathbf{a}_m = -\mathbf{a}_h$, $\mathbf{b}_m = \mathbf{a}_h + 2\mathbf{b}_h$, and $\mathbf{c}_m = -\mathbf{c}_h$, where m and h denote the monoclinic and the hexagonal cells. Because the twofold rotation $2'$ acting on the Mn_2 site results in a magnetic ion at the same position, this symmetry operation requires a sign change in the $\mathbf{b}_m$-axis spin component, and thus dictates that the in-plane component be strictly along the $\mathbf{a}_m$ or $[1,0,0]$ in the hexagonal setting. There is no constraint for the $\mathbf{b}_m$ component for Mn_1. In addition, nonzero $\mathbf{c}_m$ components are allowed at both sites. The magnetic structure of $Mn_3Si_2Te_6$ was previously reported to be a collinear spin order; the moments reside in the basal plane forming a ferrimagnetic order with strong easy-plane anisotropy [12]. However, the magnetization measurement with field $H \parallel c$ shows a continuous growth of the intensity suggesting a rather soft spin component in the c axis, although the anisotropy field is approximately 13 T [10]. A strong angular-dependent CMR with seven orders of magnitude drops in resistivity in $Mn_3Si_2Te_6$, which was first reported in Ref. [10] and later confirmed in Ref. [15], prompts a thorough reexamination of the spin configuration.

Figure 1(c) shows the temperature (T) dependence of the $(1,0,0)$ reflection that clearly exhibits an enhancement in amplitude below $T_c \approx 78$ K. A detailed comparison of wave-vector scans through the same peak at 10 and 120 K further confirms the extra magnetic scattering intensity is about 10% of the nuclear one. The coherent magnetic scattering intensity probes the spin component $\mathbf{S}_\perp$ perpendicular to the momentum transfer $\mathbf{Q}$, $\mathbf{S}_\perp = \hat{\mathbf{Q}} \times (\mathbf{S} \times \hat{\mathbf{Q}})$. The fact that additional intensity at $\mathbf{Q} = (1, 0, 0)$ appears below the transition indicates the presence of a spin component perpendicular to the $[1,0,0]$ vector. This could suggest a canted spin configuration which can be quantitatively characterized from the refinement. To do so, we perform a full $360°$ map at 5, 100, and 200 K using the white beam single crystal diffractometer CORELLI [20]. The crystal was rotated along the vertical axis with $2°$ steps between runs. Each reflection is collected with averaged redundancy of 5. Proper Lorentz, time-of-flight spectrum, and detector efficiency corrections are applied by the method detailed in Ref. [21]. A total of ≈ 500 reflections are obtained for a simultaneous refinement for the magnetic and nuclear structure using the JANA2006

TABLE I. Refined magnetic moments of symmetry independent atoms. Mn_1 is located at $(1/3, 2/3, z)$, and Mn_2 is located at $(1/3, 2/3, 1/4)$ in SG 163, $P\bar{3}1c$. The magnetic space group $C2'/c'$ puts no constraint on Mn_1 but $m_b = 0$ for Mn_2. m_a, m_b, m_c, and $|m|$ denote the amplitude of spin components along the monoclinic a_m, b_m, and c_m axes, and the total moment, respectively. Three twin domains are present with a volume ratio of 36:34:30.

Label	Multiplicity	m_a	m_b	m_c	$|m|$
Mn_1	4	−3.42(9)	1.50(8)	0.95(3)	4.55(3)
Mn_2	2	4.13(8)	0	−0.73(3)	4.20(3)

program [22]. Table I shows the refined parameters; the final spin structure is illustrated in Fig. 1(a). Both Mn sites form $\approx 10°$ canting angles toward the c axis. The nearly antiparallel Mn1 and Mn2 spins imply a considerable AFM interaction in between. Since the in-plane component of Mn_1 does not have the same constraint as Mn_2, the projected view in the ab plane shows a noncollinearity of the overall spin configuration [Fig. 1(b)].

More details on the magnetic structure are characterized near and above the transition. In contrast to the long-range order showing sharp magnetic reflections in the (H, H, L) plane [Fig. 2(a)], notable magnetic diffuse scattering exists at the magnetic peaks (0,0,2) and (1,1,2) and equivalent reflections where the Miller indices are dominant by L component [Fig. 2(b)]. This reveals a considerable in-plane spin fluc-
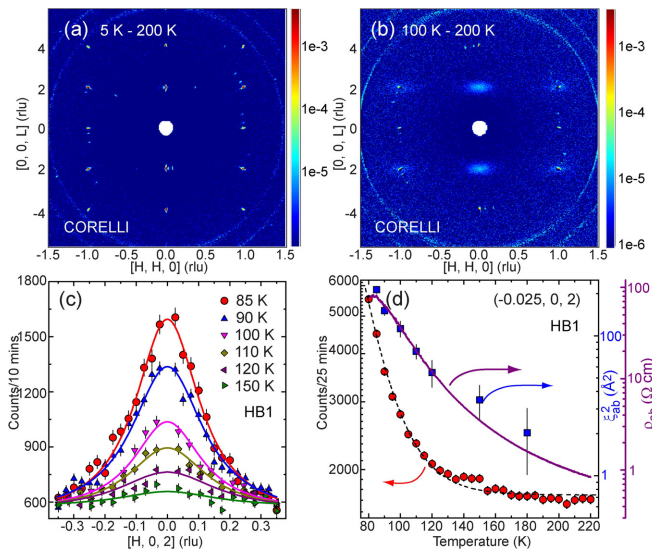

FIG. 2. (a) The contour plot of the neutron diffraction data in the (H, H, L) scattering plane collected on CORELLI at 5 K with 200-K data subtracted as background. (b) The similar plot at 100 K. (c) Wave-vector scans along the [1,0,0] direction across the magnetic (0,0,2) peak at selected temperatures. The solid lines are the Lorentzian fits to the data points. (d) Left: The T dependence of the peak intensities at $\mathbf{Q} = (-0.025, 0, 2)$. The dashed line is the fit to the data points using exponential decay form $I(T) = A_1 e^{-(T-T_0)/t_1} + I_0$, with $T_0 = 79(1)$, $t_1 = 16.3(5)$, $A_1 = 3800(20)$, and $I_0 = 1720(15)$. Right: The thermal evolution of in-plane resistivity $\rho_{ab}(T)$ (solid purple line) and $\xi_{ab}^2(T)$, where ξ_{ab} (blue solid square) is in-plane correlation length.
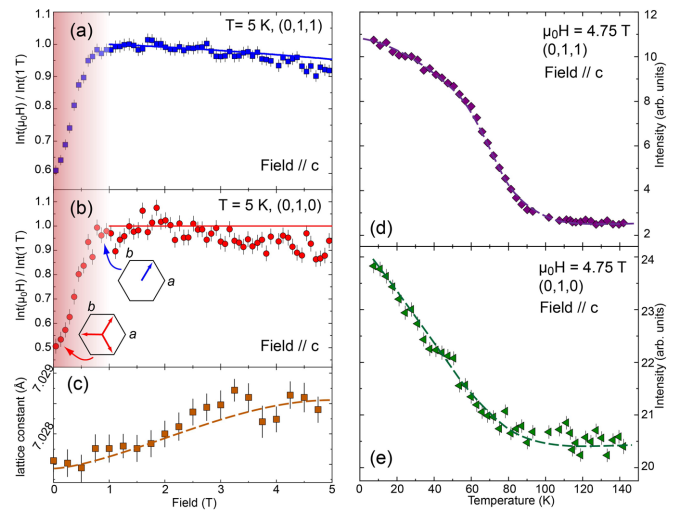

FIG. 3. Field dependence of the (a) (0,1,1) and (b) (0,1,0) magnetic reflections with field direction parallel to the c axis. Solid blue and red lines for $\mu_0 H > 1$ T are the calculated intensities with angle tilting smoothly from $10°$ to $33°$. The inset of (b) illustrates the conversion of three equally populated magnetic twins into a single domain at field ≈ 1 T. (c) The field dependence of the in-plane lattice constant a at 5 K. The temperature dependence of peak intensity of the (d) (0,1,1) and (e) (0,1,0) peaks at a field of 4.75 T. Dashed lines are guides to the eye.

tuation that can only be probed by the momentum transfer perpendicular to the spin component. The in-plane magnetic fluctuations are slightly broadened compared to those along the c axis yet maintain a three-dimensional character. Surprisingly, the diffuse scattering is present over a broad range of temperature near the transition. It peaks at the transition and persists well above T_c (Supplemental Material [13]). As shown in Fig. 2(d), peak intensities collected at $\mathbf{Q} = (-0.025, 0, 2)$ exhibit a slow decay as the temperature is raised. The intensity remains finite at temperatures close to $\approx 2T_c$. The wave-vector-dependent susceptibility above the transition can be described in the Ornstein-Zernike form $\chi(q) = 1/(q^2 + k^2)$, where $k = 1/\xi$ is the inverse correlation length. The in-plane correlation length $\xi_{ab}(T)$ displays a similar suppression on warming from 14.5(5) Å at 85 K to 4(1) Å at 180 K. These values are rather small and comparable with the in-plane lattice parameter, highlighting the confinement of the magnetic clusters above the transition. Interestingly, the thermal evolution of the ξ^2 overlaps nicely with that of the electric resistivity, which has important implications for the magnetoresistance in that temperature regime as discussed below.

We now turn to the response of the spin structure with magnetic field applied along the c axis. The full data sets are collected at 0, 1, and 4.75 T to determine the spin order, while more detailed field dependence studies are performed focusing on representative reflections of (0,1,1) and (0,1,0). As shown in Figs. 3(a) and 3(b), both peak intensities exhibit abrupt enhancement in the small field regime (<1 T). The refinement at 1 T indicates a melting of the domain walls between three nearly equally populated magnetic twins, leading to a single domain with no change in the magnetic structure.

More importantly, the data indicate that the Mn_1 ion carries a magnetic moment of 4.5 μ_B whereas the moment at the Mn_2 site is 4.2 μ_B. Therefore, the net magnetic moment, according to the magnetic configuration in Fig. 3(a), is 1.6 μ_B/Mn (equal to $[2 \times 4.5 - 4.2]/3$). This is perfectly consistent with the saturated magnetization of 1.56 μ_B/Mn in the basal plane at $\mu_0 H > 0.1$ T [10,15]. We note there is a slight misalignment of the crystal orientation where the applied field deviates from the crystalline c axis by 3°, which translates into an in-plane field $\sin(3°) \times 1$ T=0.05 T (close to 0.1 T) that overcomes the coercive field.

Further increasing the magnetic field along the c axis systematically suppresses the intensity of both (0,1,1) and (0,1,0) reflections [Figs. 3(a) and 3(b)]. Such behavior is distinct from that of the low-field regime and signals a gradual change in the spin configuration once the system enters the single domain state. In particular, the refinement reveals a further tilting of all spins toward the c axis from 10° at 1 T to 33° at 4.75 T (Supplemental Material [13]). This is illustrated by the solid lines in Figs. 3(a) and 3(b) showing evolution of the calculated intensities with spin moment tilting away from the basal plane, which capture the trend reasonably well. The in-plane lattice parameter a shows a monotonic increase with field applied along the c axis. An accurate determination of the field dependence of the c lattice parameter is not possible since the crystal is oriented with the c axis aligned out of the plane. We also measured the thermal evolution of both magnetic reflections at $\mu_0 H = 5$ T. In contrast to the sharp anomaly observed in zero field, the transition is significantly broadened. This is expected for a ferrimagnet, because the applied magnetic field forces the spins to be aligned with H above the intrinsic magnetic transition.

The magnetic response to the applied magnetic field described above makes the observed CMR with seven orders of magnitude drops in resistivity in $Mn_3Si_2Te_6$ indeed exceptional [10]. Seo *et al.* propose that the main mechanism driving an insulator-metal transition is the magnetic valve effect, where the spin rotation by external fields drastically reduces the electronic band gap and the charge conduction [15]. In light of the neutron diffraction data presented in Figs. 1–3, such a proposal becomes inadequate to explain the observed CMR. This is because our neutron diffraction results reveal that $Mn_3Si_2Te_6$ already possesses a canted angle of 10° away from the *ab* plane at ambient condition, and the canting angle changes merely to 33° at the applied field of 4.75 T along the c axis. Yet, the CMR abruptly takes place at a critical field $\mu_0 H_c = 3$ T, much smaller than the saturation field of 13 T transforming spins to a fully polarized state [Fig. 4(a)]. The lack of a parallel response to H in ρ_{ab} and the magnetic canting confirms that the magnetic spins alone cannot account for the observed CMR. Furthermore, a dramatic change in the electric conductivity is observed with application of an in-plane electric current [Fig. 4(b)]. With increasing current from 0.1 to 4 mA, the resistivity at 6 K drops by half, yet the *in situ* neutron diffraction measurement shows disproportionally small change in magnetic order. The intensity of the magnetic (0,0,2) peak reduces by 15% while T_c shifts only slightly to 75 K at 4 mA. More dramatic change in the transport properties and complex phase transitions are observed under small in-plane direct current density [23]. These observations
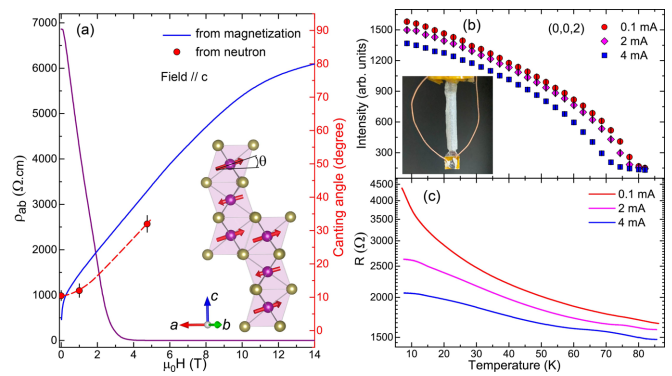

FIG. 4. (a) Field dependence of the in-plane resistivity ρ_{ab} (purple) and canted angle obtained from neutron diffraction and magnetization measurements. (b) T dependence of the (0,0,2) magnetic reflection as a function of increasing in-plane electric current. (c) The *in situ* measurement of resistance under the same experimental configuration. Inset: The setup that performs simultaneous neutron diffraction and electric transport measurement.

clearly imply that magnetoresistance in $Mn_3Si_2Te_6$ is rather complicated and different mechanisms have to be invoked.

In the low carrier density semiconductors $Tl_{2-x}Sc_xMn_2O_7$ [5–7] and $Eu_{1-x}Gd_xSe$ [24], the coupling between itinerant electrons and the fluctuating magnetic spins are emphasized as the main source contributing to resistance in the regime above T_c [8,9]. According to the model, the magnetotransport in the low carrier concentration limit ($n \leqslant 1/\xi^3$, with ξ the magnetic correlation length) ferromagnet is governed by the scattering process of the electron gas coupled to spin fluctuation. The resistivity ρ can be derived as $\rho \sim \xi^2/(1 + \xi^2 q^2)$ in the Ornstein-Zernike approximation, with q being the momentum transfer of the ferromagnetic fluctuations [25]. It is evident that $\rho \sim \xi^2$ for the low electron density situation over a wide range of temperature above the transition. The strength of the coupling constant C between the itinerant electrons and local moment can be estimated from $\Delta\rho(H)/\rho = C(m(H)/m_{sat})^2$, where $m(H)$ and m_{sat} are field-induced and saturation magnetization, and usually exhibits anomalous large values in the fluctuation scenario.

Indeed, $Mn_3Si_2Te_6$ displays a number of characteristics of the magnetic semiconductors exhibiting CMR driven by spin fluctuation; the charge carrier density is low at 10^{-4} per formula unit, which is similar to $Tl_2Mn_2O_7$ ranging from 0.001 to 0.005 [7], but significantly smaller than in doped $La_{1-x}Sr_xMnO_3$ [26]. The constant C is 105 above T_c [10], nearly two orders of magnitude higher than those in the metallic manganites [27]. Third, just like the magnetoresistivity that extends to temperature much higher than the transition, the magnetic diffuse scattering also persists at high temperature [Fig. 2(d)], revealing a close connection between the two. The square of magnetic correlation lengths of the fluctuating spins follows the thermal evolution of the resistivity. This is in line with the theoretical model that $\rho \sim \xi^2$ even with $d\rho/dT < 0$ [8,9] and the observation of a polaronic transport behavior above the transition [18]. Finally, the density function theory calculation [12] reveals that the magnetic exchange interactions are dominated by the strongest nearest

neighbor coupling J_1 along the c axis, followed by two weaker terms J_2 and J_3 perpendicular to the c axis [inset of Fig. 1(a)]. Such calculation was recently verified by spin wave excitation study using inelastic neutron scattering, which further reveals exchange anisotropy due to the spin-orbit coupling at the Mn1 site [14]. The system is frustrated because the first three magnetic exchange constants are of the same AFM type. This explains the rather low transition $T_c \approx 78$ K comparing to a much higher Curie-Weiss temperature $\Theta_{CW} \approx -277$ K and the prevailing magnetic fluctuation. With magnetic field applied along the c axis, the in-plane lattice constant shows gradual expansion upon increased field [Fig. 3(c)]. This in-plane lattice expansion could result from the magnetostriction effect and shows an opposite trend comparing to temperature dependence of the lattice constant in zero applied field [12], which conceivably might lead to modification of existing magnetic exchange interactions and eventual suppression of the magnetic frustration.

In summary, our neutron diffraction study reveals a canted spin configuration at 5 K that is crucial to understanding the unconventional CMR in the ferrimagnetic $Mn_3Si_2Te_6$. A slow and gradual spin rotation toward the c axis occurs with increasing magnetic field applied along the same direction. Our results provide direct evidence that the modification in spin order is not sufficient to explain the giant magnetoresistance response when the field is applied along the spin hard axis, and prompt further experimental [28] and theoretical efforts to describe the novel magnetotransport behavior. On the other hand, the prominent short-range magnetic diffuse scattering near T_c, the close connection between the square of spin-spin correlation lengths and electric resistivity, strongly suggests the relevance of fluctuating moments near the magnetic transition contributing to the transport properties in this low carrier density semiconductor. A future single crystal magnetic diffuse scattering study under applied field is highly desirable to provide important insight into the role of the fluctuating spins.

---

[1] S. Jin, T. H. Tiefel, M. McCormack, R. A. Fastnacht, R. Ramesh, and L. H. Chen, Thousandfold change in resistivity in magnetoresistive La-Ca-Mn-O films, Science **264**, 413 (1994).

[2] C. Zener, Interaction between the d-shells in the transition metals. II. Ferromagnetic compounds of manganese with perovskite structure, Phys. Rev. **82**, 403 (1951).

[3] P. W. Anderson and H. Hasegawa, Considerations on double exchange, Phys. Rev. **100**, 675 (1955).

[4] P. G. de Gennes, Effects of double exchange in magnetic crystals, Phys. Rev. **118**, 141 (1960).

[5] Y. Shimakawa, Y. Kubo, and T. Manako, Giant magnetoresistance in $Tl_2Mn_2O_7$ with the pyrochlore structure, Nature (London) **379**, 53 (1996).

[6] M. A. Subramanian, B. H. Toby, A. P. Ramirez, W. J. Marshall *et al.*, Colossal magnetoresistance without Mn^{3+}/Mn^{4+} double exchange in the stoichiometric pyrochlore $Tl_2Mn_2O_7$, Science **273**, 81 (1996).

[7] A. P. Ramirez, Large enhancement of magnetoresistance in $Tl_2Mn_2O_7$: Pyrochlore versus perovskite, Science **277**, 546 (1997).

[8] P. Majumdar and P. Littlewood, Magnetoresistance in Mn Pyrochlore: Electrical Transport in a Low Carrier Density Ferromagnet, Phys. Rev. Lett. **81**, 1314 (1998).

[9] P. Majumdar and P. B. Littlewood, Dependence of magnetoresistivity on charge-carrier density in metallic ferromagnets and doped magnetic semiconductors, Nature (London) **395**, 479 (1998).

[10] Y. Ni, H. Zhao, Y. Zhang, B. Hu, I. Kimchi, and G. Cao, Colossal magnetoresistance via avoiding fully polarized magnetization in the ferrimagnetic insulator $Mn_3Si_2Te_6$, Phys. Rev. B **103**, L161105 (2021).

[11] R. Rimet, C. Schlenker, and H. Vincent, A new semiconducting ferrimagnet: A silicon manganese telluride, J. Magn. Magn. Mater. **25**, 7 (1981).

[12] A. F. May, Y. Liu, S. Calder, D. S. Parker, T. Pandey, E. Cakmak, H. Cao, J. Yan, and M. A. McGuire, Magnetic order and interactions in ferrimagnetic $Mn_3Si_2Te_6$, Phys. Rev. B **95**, 174440 (2017).

[13] See Supplemental Material at http://link.aps.org/supplemental/10.1103/PhysRevB.106.L180402 for further details of crystal and magnetic structure analysis in zero and applied field and characterization of diffuse scattering across the transition.

[14] G. Sala, J. Y. Y. Lin, A. M. Samarakoon, D. S. Parker, A. F. May, and M. B. Stone, Ferrimagnetic spin waves in honeycomb and triangular layers of $Mn_3Si_2Te_6$, Phys. Rev. B **105**, 214405 (2022).

[15] J. Seo, C. De, H. Ha, J. E. Lee, S. Park, J. Park, Y. Skourski, E. S. Choi, B. Kim, G. Y. Cho, H. W. Yeom, S.-W. Cheong, J. H. Kim, B.-J. Yang, K. Kim, and J. S. Kim, Colossal angular magnetoresistance in ferrimagnetic nodal-line semiconductors, Nature (London) **599**, 576 (2021).

[16] Y. Liu and C. Petrovic, Critical behavior and magnetocaloric effect in $Mn_3Si_2Te_6$, Phys. Rev. B **98**, 064423 (2018).

[17] H. Vincent, D. Leroux, and D. Bijaoui, Crystal structure of $Mn_3Si_2Te_6$, J. Solid State Chem. **63**, 349 (1986).

[18] Y. Liu, Z. Hu, M. Abeykoon, E. Stavitski, K. Attenkofer, E. D. Bauer, and C. Petrovic, Polaronic transport and thermoelectricity in $Mn_3Si_2Te_6$ single crystals, Phys. Rev. B **103**, 245122 (2021).

[19] N. V. Belov, N. N. Neronova, and T. S. Smirnova, Shubnikov groups, Kristallografiya **2**, 315 (1957).

[20] F. Ye, Y. Liu, R. Whitfield, R. Osborn, and S. Rosenkranz, Implementation of cross correlation for energy discrimination on the time-of-flight spectrometer CORELLI, J. Appl. Crystallogr. **51**, 315 (2018).

[21] T. M. Michels-Clark, A. T. Savici, V. E. Lynch, X. Wang, and C. M. Hoffmann, Expanding Lorentz and spectrum corrections to large volumes of reciprocal space for single-crystal

time-of-flight neutron diffraction, J. Appl. Crystallogr. **49**, 497 (2016).

[22] V. Petříček, M. Dušek, and L. Palatinus, Crystallographic computing system JANA2006: General features, Z. Kristallogr. Kristallgeom. Kristallphys. Kristallchem. **229**, 345 (2014).

[23] Y. Zhang, Y. Ni, H. Zhao, S. Hakani, F. Ye, L. DeLong, I. Kimchi, and G. Cao, Control of chiral orbital currents in a colossal magnetoresistance material, Nature (London) (2022), doi: 10.1038/s41586-022-05262-3.

[24] S. Von Molnar and S. Methfessel, Giant negative magnetoresistance in ferromagnetic Eu$_{1-x}$Gd$_x$Se, J. Appl. Phys. **38**, 959 (1967).

[25] M. E. Fisher and J. S. Langer, Resistive Anomalies at Magnetic Critical Points, Phys. Rev. Lett. **20**, 665 (1968).

[26] A. P. Ramirez, Colossal magnetoresistance, J. Phys.: Condens. Matter **9**, 8171 (1997).

[27] Y. Tokura, A. Urushibara, Y. Moritomo, T. Arima, A. Asamitsu, G. Kido, and N. Furukawa, Giant magnetotransport phenomena in filling-controlled Kondo lattice system: La$_{1-x}$Sr$_x$MnO$_3$, J. Phys. Soc. Jpn. **63**, 3931 (1994).

[28] J. Wang, S. Wang, X. He, Y. Zhou, C. An, M. Zhang, Y. Zhou, Y. Han, X. Chen, J. Zhou, and Z. Yang, Pressure engineering of colossal magnetoresistance in the ferrimagnetic nodal-line semiconductor Mn$_3$Si$_2$Te$_6$, Phys. Rev. B **106**, 045106 (2022).